Ecological Engineering 74 (2015) 327–336

Contents lists available at ScienceDirect

Ecological Engineering

journal homepage: www.elsevier.com/locate/ecoleng

Saturation-excess and infiltration-excess runoff on green roofs

Wen-Yu Yang [a], Dan Li [b], Ting Sun [a,*], Guang-Heng Ni [a]

[a] State Key Laboratory of Hydro-Science and Engineering, Department of Hydraulic Engineering, Tsinghua University, Beijing 100084, China
[b] Program of Atmospheric and Oceanic Sciences, Princeton University, Princeton, NJ 08544, United States

ARTICLE INFO

Article history:
Received 10 July 2014
Received in revised form 2 October 2014
Accepted 9 October 2014
Available online 5 November 2014

Keywords:
Green roof
Rainwater retention
Saturation excess
Infiltration excess
Rainfall-runoff relationship
HYDRUS-1D

ABSTRACT

Green roofs (GRs), as compared to conventional roofs, can retain a considerable amount of water in the soil layer and hence have been used in many urban areas to mitigate urban flooding. However, a simple yet physical model for describing the rainfall (P)-runoff (R) relationship over GRs is still lacking. In this study, a physically-based P–R relationship, which utilizes soil moisture measurements that are often available in field experiments, is proposed based on the water balance equation over flat and horizontally homogenous GRs and evaluated against field measurements. First, the two different runoff generation mechanisms on GRs, namely, saturation-excess (runoff is generated when the soil becomes saturated) and infiltration-excess (runoff is generated when the rainfall intensity is larger than the infiltration rate), are discussed. A water balance analysis is then performed to obtain a physically-based P–R relationship over flat and horizontally homogenous GRs, which is validated using measurements from a field experiment conducted over a GR site in Beijing, China. Results show that our P–R relationship is able to estimate the runoff generated on our GR site. The proposed P–R relationship is also tested against other observational data and empirical models in the literature and shows broad consistency with these previous studies. To further quantify the relative importance of saturation-excess runoff and infiltration-excess runoff, numerical simulations are carried out using HYDRUS-1D. The simulation results indicate that runoff at our GR site is generated by both saturation-excess and infiltration-excess. Nonetheless, the infiltration-excess runoff accounts for a small portion of the total runoff, which suggests that the saturation-excess mechanism is more important for generating runoff over GRs.

1. Introduction

The worldwide rapid urbanization in recent years leads to significant increases in impervious (built) surfaces and concomitant reductions in green spaces. Due to these modifications in cities, various environmental issues occur, of which urban flooding is particularly detrimental. For example, Beijing, the capital city of China, has experienced several serious flooding events over the past decade. The most recent one occurred on July 21, 2012 and resulted in 79 deaths and an economic loss of ¥11.64 billion ($1.9 billion) (Zhang et al., 2013). In order to mitigate urban flooding, different strategies such as retention ponds, rainwater tanks and green roofs (GRs) have been proposed and studied (Mentens et al., 2006; Tillinghast et al., 2013). Among these strategies, the GR strategy features low impact development by utilizing the free rooftop spaces and becomes particular popular in North America (see e.g. Carson et al., 2013; Carter and Rasmussen, 2006; DeNardo et al., 2005; Mentens et al., 2006; Volder and Dvorak, 2014), Europe (see e.g. Fassman-Beck et al., 2013; Fioretti et al., 2010; Palla et al., 2011; Stovin et al., 2012; Teemusk and Mander, 2007), and East Asia (see e.g. Jim and Peng, 2012).

A typical GR usually consists of several layers, namely, a vegetation layer, a medium layer, a filtering-drainage layer, and a roof deck layer; while a typical conventional roof only has a roof deck layer. GRs are usually classified as extensive or intensive according to the medium layer depth: GRs with medium layer depth larger than 15 cm are classified as intensive GRs while those with medium layer depth less than 15 cm are extensive GRs (Carson et al., 2013). Previous studies have found that GRs can retain 27%–81% of the total rainfall and delay the runoff peak by 10 min relative to the precipitation peak (Getter et al., 2007 Mentens et al., 2006; Morgan et al., 2013; Simmons et al., 2008; VanWoert et al., 2005). However, the hydrological behavior of GRs varies across different sites due to different climates, different structure and properties of GRs, as well as different vegetation. A review of studies that focus on the impacts of these factors on the hydrological behavior of GRs is provided in Table 1.

To describe the hydrological behavior of GRs, field experiments and/or numerical simulations are usually conducted. Experimental studies usually try to construct empirical relationships between

* Corresponding author. Tel.: +86 13381105136.
E-mail address: sunting@tsinghua.edu.cn (T. Sun).

http://dx.doi.org/10.1016/j.ecoleng.2014.10.023
0925-8574/

Table 1
A review of studies that investigated the impacts of different factors on the hydrological behavior of GRs.

	Reference	Results summary
Climate conditions	Stovin et al. (2012)	GR provides 50.2% cumulative annual rainfall retention, with a total volumetric retention equivalent to 30% during the significant events.
	Carter and Rasmussen (2006)	An inverse relationship is observed between the depth of rainfall and the percentage of rain that was retained: for small storms (<25.4 mm), 88% is retained; for medium storms (25.4–76.2 mm), more than 54% is retained; and for large storms (>76.2 mm), 48% is retained.
	Mentens et al. (2006); Villarreal (2007)	The retention of GR depends on the season: the warm season (summer) results in higher evapotranspiration and the GR retention capacity regenerates faster.
	Villarreal and Bengtsson (2005)	Climate conditions (dry or wet) affect the retention capacity of GR: in the dry conditions, 6–12 mm rain water is required to initiate runoff, whereas in wet conditions, the response is almost spontaneous.
	Voyde et al. (2010)	Antecedent dry days have the greatest influence on retention. Seasonal differences do not influence runoff response in Auckland's sub-tropical climate.
Structure and soil properties	VanWoert et al. (2005); Uhl and Schiedt (2008); Morgan et al. (2013)	The layer depth dominates the retention effect as compared to other construction details. Steeply sloped roofs tend to increase runoff but only marginally.
	Volder and Dvorak (2014)	Drier green roof substrate provided additional retention benefits for larger rain events.
	Farrell et al. (2013)	Water-retention additives can increase substrate water availability: silicates increased water holding capacity in both scoria and roof-tile substrates, but hydrogel only improved scoria water holding capacity.
	Voyde et al. (2010)	No statistically significant differences were found between the substrate types tested (i.e. clay, zeolite and pumice).
Vegetation	Dunnett et al. (2008b); Monterusso et al. (2004); VanWoert et al. (2005)	The vegetation type and cover do not significantly affect the water retention of GR.
	Steusloff (1998); Wolf and Lundholm (2008); Schroll et al. (2011)	The vegetation plays an important role in water retention, especially in periods with low water availability and higher temperatures.
	Nagase and Dunnett (2012)	A significant difference in amount of water runoff is observed among GRs with different vegetation types.
Review	Czemiel Berndtsson (2010)	This paper provides a review of studies on GR's hydrological behaviors.

runoff characteristics (e.g. runoff amount, runoff delay, peak runoff reduction, etc.) and rainfall characteristics (e.g. precipitation amount, rainfall duration, rainfall intensity, etc.) on an event-to-event basis (Carson et al., 2013; Carter and Jackson, 2007; Fassman-Beck et al., 2013; Mentens et al., 2006; Palla et al., 2012; Stovin et al., 2012). For example, some studies proposed quadratic models to link the amount of runoff to the amount of rainfall (as will be discussed later in Fig. 4). These empirically-based *P*–*R* relationships are based on regression analyses and thus lack physical interpretations. As a result, their applications are limited to places where the regression analyses are conducted. As compared to these empirical relationships, models based on water balance have been proposed by many researchers. For example, simple hydrological models such as the one proposed by Stovin et al. (2013) can perform long-term, continuous simulations to estimate runoff and evaluate drought risks. Vanuytrecht et al. (2014) developed a model based on water balance at daily scales. An analytical, probabilistic model for evaluating the long-term hydrologic performance of extensive green roofs was proposed by Zhang and Guo (2013). These models are typically used at daily or monthly time scales but not on an event-by-event basis. In addition to these empirical and water-balance models, more sophisticated numerical models like HYDRUS-1D (Hilten et al., 2008) and SWMM-2D (Palla et al., 2009; Burszta-Adamiak and Mrowiec, 2013) are widely used to simulate the hydrological behavior of GRs. They have been demonstrated to perform reasonably well in simulating the hydrodynamics in GRs as long as their input parameters are well calibrated (Li and Babcock, 2014). Relatively simpler numerical models such as the Green–Ampt infiltration model are also used (e.g., She and Pang (2010)).

Although various empirical *P*–*R* relationships have been proposed in the literature, a simple yet physical one that can be used on an event-to-event basis is still lacking, which motivates this study. In particular, most field experiments measure the soil moisture at some point in the GR column but this information is usually not used when constructing the *P*–*R* relationship (see e.g. Carson et al., 2013; Fassman-Beck et al., 2013). In this study, we aim to utilize this information of soil moisture in constructing a new and potentially more general *P*–*R* relationship for typical flat and horizontally homogeneous GRs based on the water balance equation. Our new *P*–*R* relationship is thus different from those reported in the literature that are constructed based on regression analyses. Our model is also different from other models that are based on water balance (Stovin et al., 2013; Vanuytrecht et al., 2014; Zhang and Guo, 2013) since our model is applied on an event-by-event basis. We also combine both field experiments and numerical simulations to investigate the hydrological behavior of GRs and validate our *P*–*R* relationship. The paper is organized as follows: we first discuss the two different runoff generation mechanisms on GRs, namely, saturation-excess (runoff is generated when the soil becomes saturated) and infiltration-excess (runoff is generated when the rainfall intensity is larger than the infiltration rate). We then perform a water balance analysis for a typical flat and horizontally homogeneous GR and propose a relationship between the rainfall amount *P* and the runoff amount *R*. A field experiment is conducted to calibrate and validate the *P*–*R* relationship. Numerical simulations via HYDRUS-1D are carried out to further investigate the relative importance of saturation excess runoff and infiltration excess runoff and to assess the applicability of our *P*–*R* relationship.

2. Theory

2.1. Runoff generation mechanisms on GRs

In general, runoff can be generated through two different mechanisms: saturation-excess (i.e, runoff is generated when the soil becomes saturated) and infiltration-excess (i.e., runoff is generated when the rainfall intensity becomes larger than the infiltration rate of water into the soil). The following analysis (done on an event-by-event) summarizes cases with runoff generated by different mechanisms. The subscript '*k*' indicates the k^{th} event.

Depending on the total rainfall amount and the rainfall intensity during a rainfall event, there can be four different cases for runoff generation on GRs:

Case 1. $P_k \le (\theta_s - \overline{\theta}_{ik})Z_r, I_k(t) \le K_s$

where P is the total rainfall amount of the k^{th} rainfall event, I is the rainfall intensity of the k^{th} rainfall event, θ_s is the saturation water content, which is a property of the soil and hence does not vary with different rainfall events, $\overline{\theta}_i$ is the initial soil moisture averaged over the GR column before the k^{th} rainfall event, Z_r is the depth of the soil in the GR column. As such, $\left(\theta_s - \overline{\theta}_{ik}\right)Z_r$ represents the maximum water holding capacity of the soil for the k^{th} rainfall event. K_s is the saturated hydraulic conductivity, which is also a property of the soil and represents the maximum infiltration rate or the infiltration capacity of the soil. In this case, the total rainfall amount is less than the maximum water holding capacity of the GR and the rainfall intensity is always less than the maximum infiltration rate, hence all rain enters the soil and no runoff is generated.

Case 2. $P_k > (\theta_s - \overline{\theta}_{ik}Z_r,\ I_k(t) < K_s$

In this case, the total rainfall amount is larger than the maximum water holding capacity of the GR but the rainfall intensity is still always less than the maximum infiltration rate, hence runoff is only generated after the soil becomes saturated, namely, through saturation-excess.

Case 3. $P_k > \left(\theta_s - \overline{\theta}_{ik}\right)Z_r$, and $I_k(t) > K_s$ when $t_1 < t < t_2$

In this case, the total rainfall amount is larger than the maximum water holding capacity of the GR. Hence after the soil becomes saturated, runoff is generated though saturation-excess. In addition, during the period from t_1 and t_2, runoff is also generated through infiltration-excess because the rainfall intensity is larger than the maximum infiltration rate. The total runoff is the sum of infiltration-excess runoff and saturation-excess runoff.

Case 4. $P_k < \left(\theta_s - \overline{\theta}_{ik}\right)Z_r$, and $I_k(t) > K_s$ when $t_1 < t < t_2$

In this case, the total rainfall amount is smaller than the maximum water holding capacity of the GR. As a result, the soil never gets saturated (i.e., no saturation-excess generated runoff). However, during the period from t_1 and t_2, runoff is generated because the rainfall intensity I_k is larger than the maximum infiltration rate. Thus the runoff is solely generated via infiltration-excess.

2.2. A rainfall-runoff relationship from water balance analysis over a GR

In this study, an analysis of the water balance over a flat GR of depth Z_r is presented, with the aim of constructing a P–R relationship that is physically-based and utilizes the soil moisture measurements that are often available in field experiments. Assuming no lateral flow, the water balance of the GR integrated over a time interval Δt is:

$$\Delta S = P - LE - R, \tag{1}$$

or,

$$\frac{\Delta S}{P} = \frac{P - LE - R}{P} = 1 - \frac{LE}{P} - \frac{R}{P}, \tag{2}$$

where $\Delta S = \int_0^{Z_r} (\theta_e - \theta_i)dz$ is the change in soil water content integrated over the GR column, P is the total rainfall amount, LE is the evapotranspiration, and R is the runoff. θ_e is the soil moisture at the end of Δt and θ_i is the soil moisture at the beginning of Δt. The depth of the GR, Z_r, is represented by the depth of the medium layer for simplicity, since our lab experiments (details can be found in the Appendix A) indicate that the water retention capability of GRs mostly relies on the medium layer.

For heavy rainfall, LE/P is likely to be very small and hence is assumed to be 0 (Klaassen et al., 1998). Eq. (2) thus reduces to:

$$\frac{\Delta S}{P} \approx 1 - \frac{R}{P}. \tag{3}$$

Let's denote that $\overline{\theta}_e$ and $\overline{\theta}_i$ are the vertically-averaged initial soil moisture and the vertically-averaged soil moisture at the end of Δt, respectively:

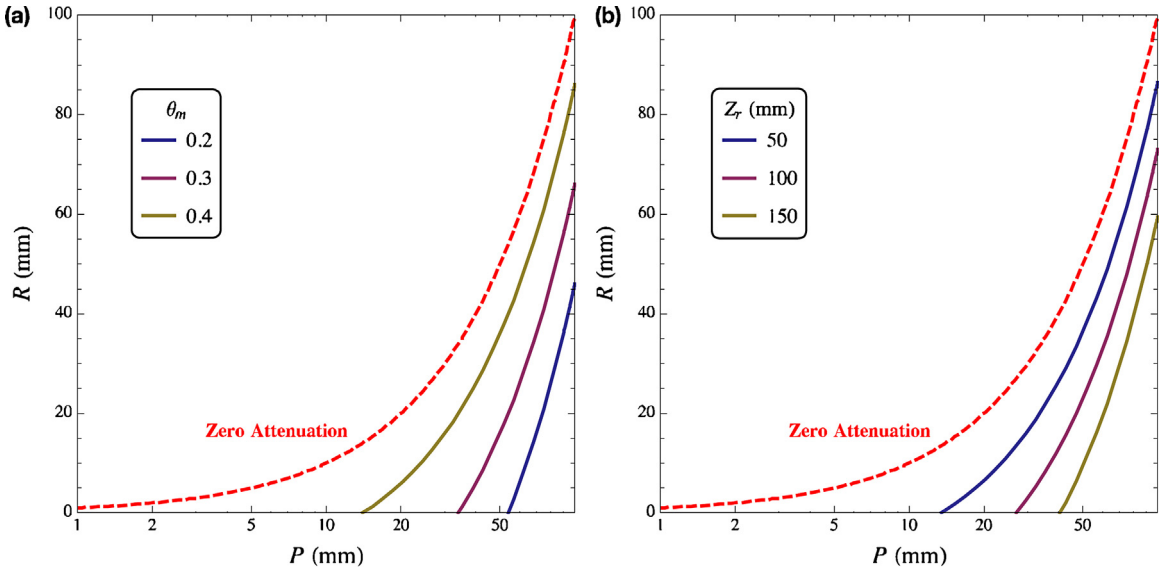

Fig. 1. Variations of runoff R from GR as a linear function of rainfall depth P with (a) different initial moisture content θ_m and (b) different medium layer depth Z_r. The red dashed line denotes the relationship between R and P under the zero attenuation scenario (i.e., $P = R$). Note that the shape factor C adopts a value of 1.0 and the field capacity is set to be 0.47 $m^3 m^{-3}$. (For interpretation of the references to color in this figure legend, the reader is referred to the web version of this article.)

$$\overline{\theta}_e = \frac{1}{Z_r}\int_0^{Z_r} \theta_e dz, \tag{4}$$

$$\overline{\theta}_i = \frac{1}{Z_r}\int_0^{Z_r} \theta_i dz, \tag{5}$$

Then the change in the soil moisture integrated over the GR column is expressed as:

$$\Delta S = \left(\overline{\theta}_e - \overline{\theta}_i\right) Z_r. \tag{6}$$

Further assuming that $\theta_e = \theta_s$ where θ_s is the saturation water content (i.e., the soil becomes saturated after raining over the time interval Δt), Eq. (6) becomes:

$$\Delta S = \left(\theta_s - \overline{\theta}_i\right) Z_r. \tag{7}$$

Let's further denote:

$$\overline{\theta}_i = \frac{1}{Z_r}\int_0^{Z_r} \theta_i dz = \theta_m C \tag{8}$$

where θ_m is the initial soil moisture measured at one single point in the column (since in field experiments, soil moisture measurements are often only available at a single point). C accounts for the variability in the vertical profile of soil water content over the GR column and is assumed to be a constant (C is called the shape factor hereinafter). In Appendix B, we examine the variability of C using numerical simulations and find that it does not vary significantly, especially at the beginning of rainfall events. Note the value of C should be on the order of 1.

Substituting Eq. (8) into Eq. (7) yields:

$$\Delta S = (\theta_s - C\theta_m) Z_r. \tag{9}$$

Combining Eq. (9) and Eq. (3) gives:

$$\frac{(\theta_s - C\theta_m) Z_r}{P} = 1 - \frac{R}{P}, \tag{10}$$

or

$$C = \frac{\theta_s - 1/Z_r(P-R)}{\theta_m} \tag{11}$$

with Eq. (11), C can be calculated for each rainfall event that generates saturation-excess runoff given measurements of rainfall, runoff and initial soil moisture at one point and the saturation water content θ_s. If θ_s is unknown, Eq. (11) can be arranged as:

$$\frac{(P-R)}{Z_r} = \theta_s - \theta_m \mathrm{C} \tag{12}$$

As such, fitting a linear relationship between $(P–R)/Z_r$ and θ_m will yield θ_s and C. This can be done during the model calibration. If

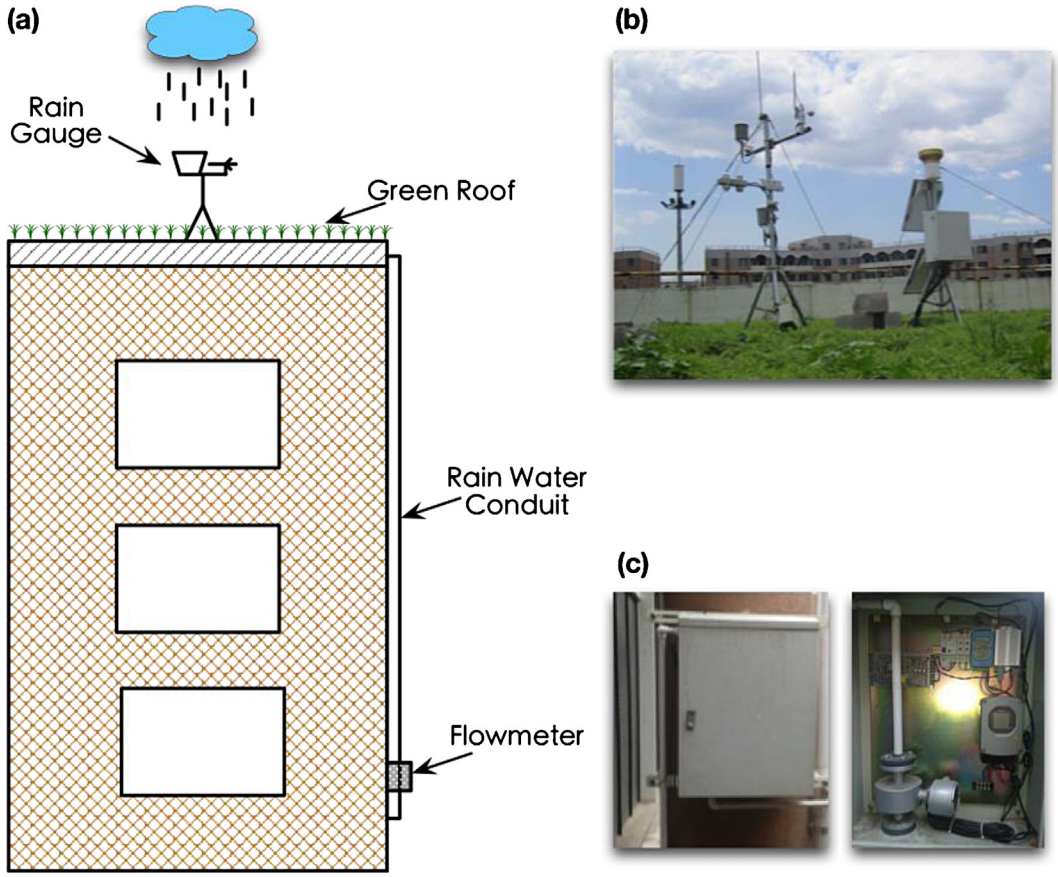

Fig. 2. Schematic overview of the field experiment conducted at a GR site on Tsinghua campus. (a) The overall layout of the onsite experiment. (b) the site view of the rain gauge and the vegetation installed on the rooftop. (c) left panel: the flowmeter box attached on the wall; right panel: the interior look of the flowmeter box with monitoring instruments installed.

Table 2
Summary of the field experiment results.

Date	Precipitation (mm)	Rainfall duration (min)	Runoff (mm)	Retention ratio (%)	Runoff delay (min)	Initial moisture content (%)
21/07/2012[a]	190.4	920	157.8	17.1	110	21.3
30/07/2012[a]	69.4	2715	53.1	23.5	17	26
24/06/2012[a]	53.4	410	5.3	90.1	181	18.6
09/07/2012[a]	52.9	320	36.7	30.6	13	27.5
27/07/2012	26.9	965	11.5	57.2	18	24.9
05/07/2012	10.5	85	0.1	99.1	1	26.1
21/04/2012	6.6	60	0	100	–	26.1
10/04/2012	2.9	70	0	100	–	17
18/04/2012	2.9	190	0	100	–	26.1
19/06/2012	2.8	120	0	100	–	18.5
25/07/2012	2.5	25	0	100	–	24.5
08/07/2012	2.2	20	0	100	–	27.4
20/04/2012	1.8	25	0	100	–	26

[a] Denotes heavy rainfall events, with rainfall depths larger than 50 mm.

we assume θ_s is a constant for a specific soil, we can also obtain θ_s from soil moisture measurements right after those rain events that have generated saturation-excess runoff. In this case, only C needs to be determined through fitting.

With θ_s and C obtained through either model calibration or measurements, a linear model between rainfall and runoff can be proposed as follows:

$$R = P - Z_r(\theta_s - \theta_m C). \quad (13)$$

It is clear that when $\theta_m = \theta_s$, $C = 1$ (i.e., the soil is already saturated at the initial stage of Δt), then $P = R$, which is expected. Fig. 1 shows the P–R relationship from Eq. (13) and how it is modulated by the initial soil moisture (represented by θ_m that is measured at some point within the GR column) and the medium layer depth (represented by Z_r). It is clear that the initial soil moisture and the medium layer depth play crucial roles in determining the P–R relationship. A higher initial soil moisture tends to reduce the water holding capability of GRs (Fig. 1a), whereas a thicker medium layer generates less runoff (Fig. 1b). This highlights the importance of considering the properties of GRs (such as the depth) and the properties of the soil (such as the initial soil moisture) in constructing the P–R relationship. Empirically-based P–R relationships that do not account for these two factors are unlikely to be applicable over different GRs.

There are three critical assumptions made in above analysis: (1) there is no lateral flow; (2) evapotranspiration is not important during the rain event; (3) the soil becomes saturated during or after the rain event. The first assumption is justified by our consideration of only flat and horizontally homogenous GRs here. Studies have shown that inclination is an important factor that can potentially alter the hydrological behavior of green roofs (Van-Woert et al., 2005; Dunnett et al., 2008a). The reason that we did not include the effect of slope in our analyses is because the slope at our site is minimal so we do not have the effect of slope in our experimental observations. The second assumption is often justifiable since evapotranspiration is often small during rainfall events due to the energy limitation as well as the reduced vapor pressure deficit. The third assumption essentially means that runoff is at least partially generated by saturation-excess, which makes the model only applicable for Cases 2 and 3 that are presented in Section 2.1. For Case 1 in Section 2.1, since no runoff is generated, there is no practical value considering the P–R relationship. For Case 4 where only infiltration-excess runoff occurs, the assumption that the soil moisture of GR becomes saturated no longer holds. As such, the model proposed here may not be applicable. In the following sections, we examine the validity of the proposed model using field experiments (Section 3.1) and numerical simulations with HYDRUS-1D (Section 3.2).

3. Results

3.1. Field experiments

To test the P–R model proposed in Section 2.1, a field experiment was conducted at a GR site located on an 11 m multi-functional office building on Tsinghua campus in Beijing, China (hereinafter the TU site). The roof has an area of 120 m^2 and a southern inclination of 3°. The thickness of the vegetation layer, medium layer and filtering-drainage layer are 5 cm, 15 cm, and 3 cm, respectively. The vegetation planted on the roof is *sedum linear*. The precipitation P, the water content θ_m in the medium layer and the runoff R are measured by a rain gauge, a TDR sensor and a flowmeter, respectively. All the instruments are connected with a data logger that samples every 10 s and records at a frequency of 5 min. The site view and the instrumentation are shown in Fig. 2. The experiment was carried out from April 1, 2012 to July 31, 2012, during which 15 rainfall events were observed (see

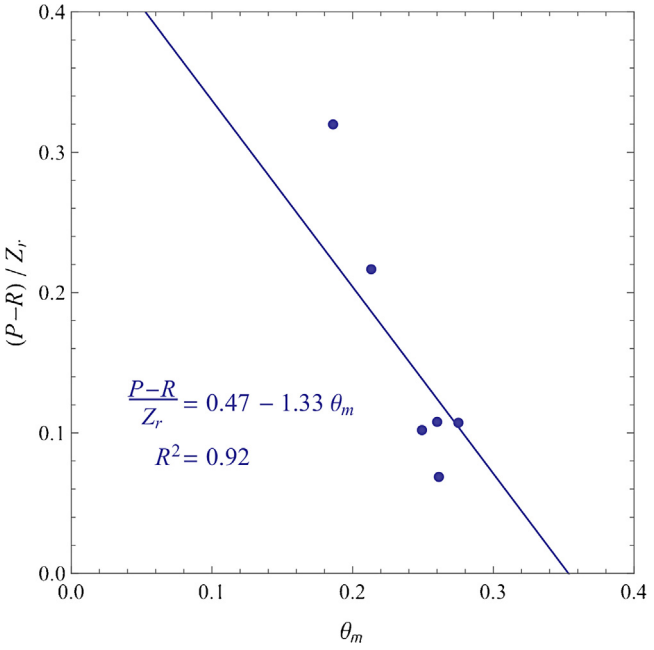

Fig. 3. Linear relationship (line) between two parameters θ_m and $(P–R)/Z_r$ fitted from observations (dots).

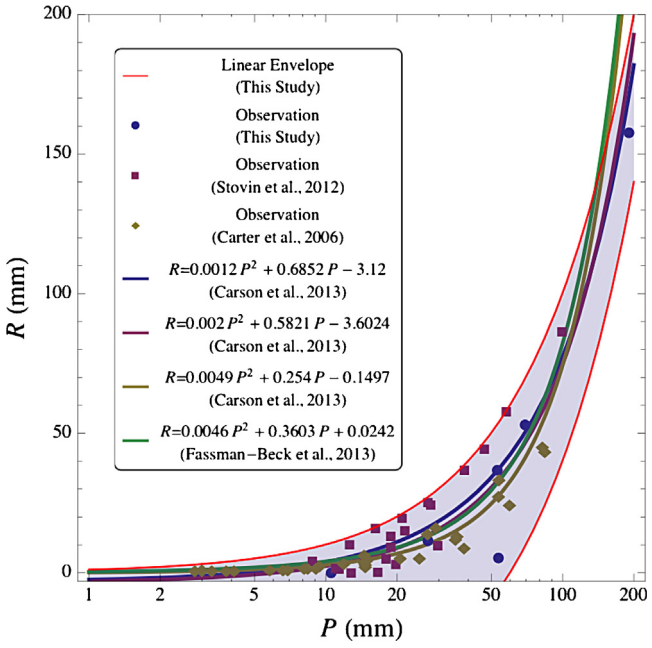

Fig. 4. Relationship between rainfall depth P and runoff R from GR from this study and other literature. The plot-markers represent observations from field experiments. The bold lines indicate various quadratic relationships between P and R calibrated in other studies. All the observations and quadratic relationships lie within the envelope indicated by the red lines. The upper and lower red lines denote the linear P–R relationships proposed by this study with a 150 mm medium layer under initial moisture contents of 0.3 $m^3\,m^{-3}$ and 0.15 $m^3\,m^{-3}$, respectively. (For interpretation of the references to color in this figure legend, the reader is referred to the web version of this article.)

Table 2), including the extreme event on July 21, 2012 that was mentioned in the introduction.

Only those events during which runoff was generated are used to study the relationship between $(P–R)/Z_r$ and θ_m, following Eq. (13). Hence Case 1 discussed in Section 2.2 is excluded from our analysis. However, at this stage, no distinction is made among the other three cases (see Section 2.2). As revealed in Fig. 3, the two parameters in Eq. (13), $(P–R)/Z_r$ and θ_m, do follow a quasi-linear relationship. The saturation water content θ_s is obtained from soil moisture measurements (not shown here) right after those rain events that have generated runoff, which is 0.47 $m^3\,m^{-3}$, whereas the shape factor C is found to be 1.33 by linear regression. It is noteworthy that the fitted value 1.33 of the shape factor C is on the order of 1, which is in agreement with our expectation. The disparity between the observations and the fitted line may result from the different initial soil moisture conditions and the uncertainties in the measurements. It should be noted that the relatively larger bias observed when $\theta_m = 0.186\,m^3\,m^{-3}$ might be attributable to the variability in the shape factor C, which varies under different soil moisture conditions.

We further compared our results to the models proposed by previous studies (Carson et al., 2013 Fassman-Beck et al., 2013) along with observational data from the literature (Carter and Rasmussen, 2006 Stovin et al., 2012), as shown in Fig. 4. Taking two values, 0.15 and 0.3, as the initial soil moisture in our model, the proposed linear model covers the region where the previously proposed quadratic models and observational data lie in. This implies that our model is in broad agreement with the models proposed by previous studies as well as other field experiments.

In practice, given that the parameters θ_s and C can be obtained or calibrated using routinely measured rainfall depth P and initial soil moisture θ_m, the hydrological behavior of a GR can be described by the model Eq. (13). It is noteworthy that the linear model is based on the assumption that the soil becomes saturated during or after the rain event but the model doesn't distinguish the saturation-excess and infiltration-excess in the total runoff. Nevertheless, as can be seen in our comparison with previous models and observational data, it seems that the linear model works reasonably well under various scenarios. To further explore the contributions of saturation-excess runoff and infiltration-excess runoff to the total runoff, an investigation using numerical simulations via HYDRUS-1D is presented in the next section.

3.2. Numerical simulations via HYDRUS-1D

HYDRUS-1D, developed by the International Groundwater Model Center (IGWMC), has been used to simulate the water and heat transport processes in porous media with a variety of sources and sinks and under a variety of boundary conditions (Šimu°nek et al., 2009). In HYDRUS-1D, the control equation of one-dimensional vertical water movement in porous media is

$$\frac{\partial\theta}{\partial t} = \frac{\partial}{\partial t}\left[D(\theta)\frac{\partial\theta}{\partial z}\right] - \frac{\partial K(\theta)}{\partial t} - S_r(z,t) \tag{14}$$

where $D(\theta)$ is the hydraulic diffusivity, $K(\theta)$ is the hydraulic conductivity, z is the soil depth, t is time, and $S_r(z,t)$ is the sink/source term.

The soil hydraulic properties are described as Van Genuchten (1980):

$$\theta(h) = \theta_r + \frac{\theta_s - \theta_r}{1 + a|h - h_a|^{\overline{n}}} \tag{15}$$

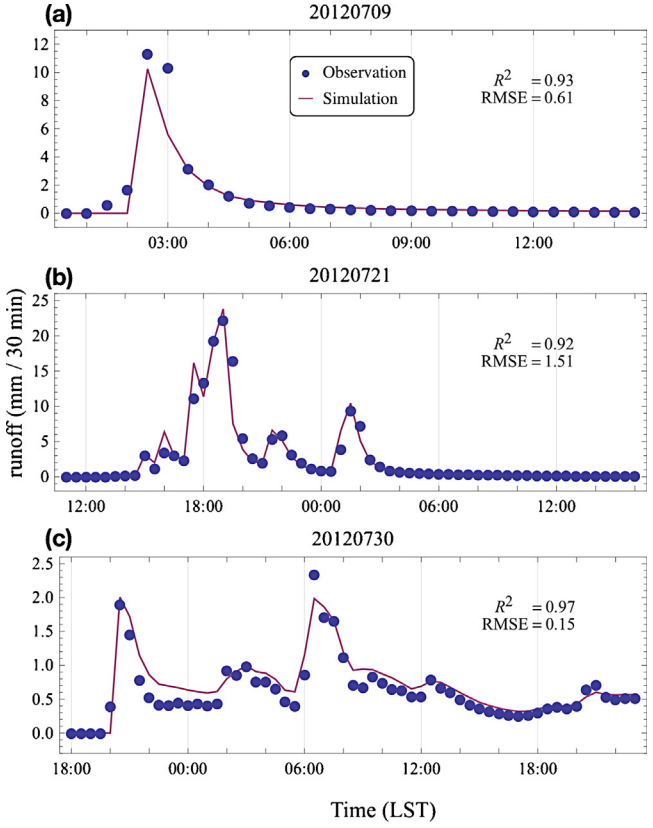

Fig. 5. Comparison of simulated runoff (red lines) and observations (blue dots) for HYDRUS-1D validation for three heavy rainfall events: (a) July 9th, 2012; (b) July 21st, 2012 and (c) July 30th, 2012. (For interpretation of the references to color in this figure legend, the reader is referred to the web version of this article.)

Table 3
Hydraulic properties of the medium layer calibrated for HYDRUS-1D simulations (the symbols have the same meaning as in Eqs. (18) and (19)).

θ_r ($m^3 m^{-3}$)	θ_s ($m^3 m^{-3}$)	α (cm^{-1})	n	K_s ($cm\,h^{-1}$)
0.176	0.469	0.03	1.3	3.6

$$K(S_e) = K_S S_e^{1/2}\left[1-\left(1-S_e^{1/m}\right)^m\right]^2 \quad (16)$$

where $S_e = (\theta-\theta_r)/(\theta_s-\theta_r)$ is the effective saturation. θ_s is the saturated soil moisture, θ_r is the residual soil moisture, h is the soil water pressure head, K_s is the saturated hydraulic conductivity as already introduced before, and n and m are two empirical parameters.

The initial conditions can be given as the moisture profile over the 1-D soil column as follows:

$$\theta(z,0) = \theta_0 \quad (17)$$

To mimic the dynamics of GR at the TU site, a medium layer with a depth of 15 cm is used in HYDRUS-1D, which is identical to that at the TU site. The hydraulic properties of the medium layer are obtained through calibration using the observations of the July 9, 2012 rainfall event at the TU site (see Fig. 5a). The properties obtained through calibration are provided in Table 3. Further validations against observations of the July 21, 2012 and July 30, 2012 rainfall events are shown in Fig. 5b and c. The RMSE and R-square demonstrate the capability of the calibrated model in capturing runoff generated from this GR.

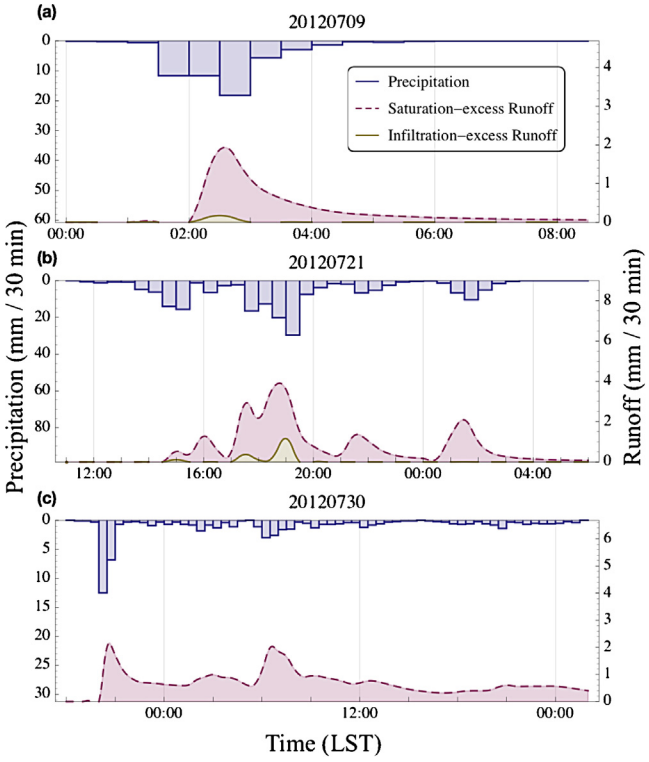

Fig. 6. Simulated saturation-excess and infiltration-excess runoffs by HYDRUS-1D for three heavy rainfall events: (a) July 9, 2012, (b) July 21, 2012 and (3) July 30, 2012. Saturation-excess and infiltration-excess runoffs from GR are represented by purple dashed and yellow solid lines, respectively. The rainfall is indicated as upper inverted bars. (For interpretation of the references to color in this figure legend, the reader is referred to the web version of this article.)

Table 4
Simulated result by HYDRUS-1D (saturation-excess, infiltration excess and total runoff are denoted by S, I, T, respectively). All in units of mm.

	09/07/2012			21/07/2012			30/07/2012		
Slope	S	I	T	S	I	T	S	I	T
0	23.3	0.9	24.2	149.2	9.8	159.0	57.5	0	57.5
5%	22.9	1.1	24.0	150.2	9.2	159.4	57.4	0	57.4
10%	22.5	1.6	24.1	146.9	11.2	158.1	57.3	0	57.3
20%	22.0	1.9	23.9	145.0	13.1	158.1	57.0	0	57.0
30%	21.2	2.5	23.7	143.6	14.8	158.4	56.8	0	56.8

Fig. 6 further separates the total runoff into runoff generated by saturation-excess and runoff generated by infiltration-excess. For the two rainfall events on July 9 and July 21, 2012, as shown in Fig. 6a and b, runoff on GR was generated by both infiltration-excess (yellow region) and saturation-excess (red region). In other words, the runoff generation mechanism on GR is in fact the combination of infiltration-excess and saturation processes. The runoff resulting from infiltration-excess only occurred during the period when the rainfall intensity was relatively large; while the runoff resulting from saturation lasts much longer. Compared to these two events, the July 30 event with lower rainfall intensity only has runoff generated from saturation-excess, as demonstrated in Fig. 6c. After quantifying the runoff generated by infiltration-excess, we found that it contributes to a small portion of the total runoff. For the July 9 event, only 3% of the total runoff is generated by infiltration-excess. Even for the July 21 event, which was the most severe storm event in the past six decades in Beijing area, the infiltration-excess runoff accounted for only 6% of the total runoff.

Despite that our GR does not have any slope, the influence of slope or inclination on the runoff generated by infiltration-excess and saturation-excess is examined using numerical simulations. As shown in Table 4, infiltration-excess is typically increased as the slope increases due to the higher potential energy. For the July 21 event, when the roof is flat, the infiltration-excess is about 6%; when the slope of the roof increases to 30%, the infiltration-excess runoff increases to 9.3% of the total runoff. As such, although there is an increase in the contribution of infiltration-excess runoff, it remains a small component of the total runoff. This result is consistent with the experiment monitoring by Uhl and Schiedt (2008). In their experiments, no direct surface runoff was observed even during high intensity rain events. The above results suggest that the saturation-excess mechanism dominates runoff generation on flat and horizontally homogenous GRs.

4. Conclusions

In this paper, a theoretical analysis of the relationship between the rainfall depth P and the runoff amount R on GRs is performed based on the soil water balance. Assuming that (1) there is no lateral flow; (2) evapotranspiration is not important during the rain event; (3) the soil becomes saturated during or after the rain event, the runoff R can be estimated from the rainfall depth P and the initial soil moisture θ_m with the saturation water content θ_s and a shape factor C obtained through calibration. The P–R relationship (i.e. Eq. (13)) can thus be employed to assess the hydrological performance of a given GR. As indicated by the proposed linear model, a thinner medium layer or a high initial soil moisture will decrease the rainwater retention capacity of GR by generating more runoff, and vise versa.

The proposed linear model is then tested with the observational data from a field experiment conducted at Tsinghua University in Beijing, China between April 2012 and July 2012. The model proved to be able to estimate runoff generated at this GR site. Further comparison of the linear model with other observational data and

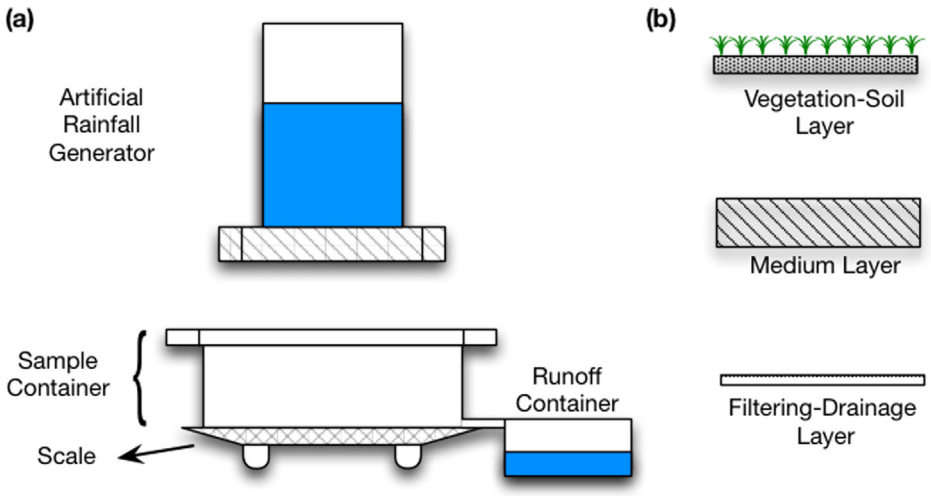

Fig. A1. Schematic overview of the lab experiment. (a) The layout of instruments for the indoor experiment. (b) Test parts to be placed in the GR container for sub-tests.

empirical models from the literature also demonstrates the applicability of the linear model under different rainfall conditions.

The contributions of saturation-excess runoff and infiltration-excess runoff to the total runoff are further quantified by numerical simulations with HYDRUS-1D. The simulations are forced by rainfall observations at TU site and include three heavy rainfall events with an extreme event on July 21, 2012. The simulation results indicate that both saturation and infiltration excess runoff occurred on our GR; nonetheless, the infiltration-excess runoff accounts for only a small portion of the total runoff. This implies that the saturation-excess mechanism dominates runoff generation on flat and horizontally homogenous GRs.

Appendix A: Hydrological performance of GR based on lab experiment

This appendix investigates the contribution of different components of GR (including the vegetation-soil layer, the medium layer, and the filtering-drainage layer) to total rainfall retention. A series of lab experiments were carried out with a GR apparatus that is shown in Fig. A1. The GR apparatus consists of an artificial rainfall generator, a sample container, a runoff collector and a weighing scale. The artificial rainfall generator produces rainfalls with different intensities and durations. The sample container is used to anchor one of the GR components (hereafter the test component). The runoff collector collects the runoff from the sample container; and the weighing scale is placed beneath the sample container for continuous measurement of the total weight of the container. The amount of retained water by the test component is the difference in the total weight of the container prior to and after the artificial rainfall. For all cases, the artificial rainfall generator is operated at rainfall intensity of 150 mm h^{-1} to simulate heavy rainfall conditions and is switched off when the runoff becomes steady.

Table A1
Summary of the lab experiment results.

Layer		Retention (mm)
Vegetation		6.8
Medium	50 mm	27.1
	150 mm	42.9
	200 mm	59.2
Filtering-drainage		2.4

The comparison of retention amounts by different components of GR is provided in Table A1. The medium layer retains most of the water and hence controls the performance of the whole GR system, which is in agreement with previous studies (Dunnett et al., 2008b; VanWoert et al., 2005). Nevertheless, it is also pointed out that approximately 1/5 of the total retention of GR is attributed to the components other than the medium layer, which remains significant.

Appendix B: Variability of the shape factor *C*

The shape factor *C* is introduced in Eq. (8) as a constant to account for the variability in the vertical profile of soil moisture in a green roof column. Due to the fact that the neighbor TDR (time domain reflectometry) sensors have to be installed at least 10 cm apart to avoid mutual inference and an extensive green roof has a depth of 15 cm or less (Carson et al., 2013), it is not feasible to obtain the profile of soil moisture by vertically installing multiple moisture sensors. As such, the variability of shape factor *C* has to be examined through ways other than direct measurements.

PROM (Princeton ROof Model) is a full-fledged hygrothermal model for simulating thermal dynamics and hydrological transport within green roof systems and its details are referred to Sun et al. (2013). The parameters and ambient forcing used in the PROM are adopted from a simulation study with PROM (Sun et al., 2014) as detailed in their Table 1. In this validation simulation, PROM is set to allow evapotranspiration on the top boundary to mimic the real scenario (or so-called online simulation).

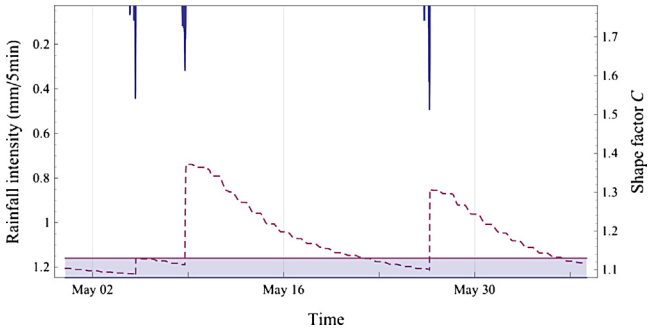

Fig. B1. Variations of shape factor *C* (dashed line) and rainfall (inverted bars). The shaded area indicates the range of antecedent-rain *C* values.

Based on the long-term online simulation results, the shape factor C is calculated according to Eq. (8) as follows

$$C = \frac{1}{\theta_m Z_r} \int_0^{Z_r} \theta_i dz \quad \text{(B1)}$$

where θ_m adopts the simulated soil moisture values at the top second level in the medium layer (referring to a depth of 9.5 cm from the top boundary), Z_r is the depth of the medium layer, and θ_i denotes the simulated soil moisture at the i-th level.

Fig. B1 shows the variations of the shape factor C from long-term online simulations. It is found that the shape factor C ranges between 1.0 and 1.4 during the simulation period and becomes stable during the antecedent dry period as indicated by the shaded area. It is also noteworthy that the shape factor C is always around 1.1 right before the onsets of rainfall, implying high confidence in taking C as a constant to estimate the vertically-averaged initial soil moisture..

Acknowledgement

This work is supported by the National Science Foundation of China under Grant No. NSFC-51190092, by China Postdoctoral Science Foundation under Grant No. 2014M550070 and by the Ministry of Science and Technology of China under Grant No. 2013DFG72270. We are grateful to the Tsinghua Property Management Center for the assistance in field measurements.

References

Burszta-Adamiak, E., Mrowiec, M., 2013. Modelling of green roofs' hydrologic performance using EPA's SWMM. Water Sci. Technol. 68 (1), 36–42.
Carson, T.B., Marasco, D.E., Culligan, P.J., McGillis, W.R., 2013. Hydrological performance of extensive green roofs in New York City: observations and multi-year modeling of three full-scale systems. Environ. Res. Lett. 8, 24,036. doi:http://dx.doi.org/10.1088/1748–9326/8/2/024036.
Carter, T., Jackson, C.R., 2007. Vegetated roofs for stormwater management at multiple spatial scales. Landscape Urban Plan. 80, 84–94. doi:http://dx.doi.org/10.1016/j.landurbplan.2006.06.005.
Carter, T., Rasmussen, T.C., 2006. Hydrologic behavior of vegetated roofs. J. Am. Water Resour. Assoc. 42, 1261–1274. doi:http://dx.doi.org/10.1111/j 1752–1688.2006.tb05299.x.
Czemiel Berndtsson, J., 2010. Green roof performance towards management of runoff water quantity and quality: a review. Ecol. Eng. 36 (4), 351–360.
DeNardo, J., Jarrett, A., Manbeck, H., Beattie, D., Berghage, R., 2005. Stormwater mitigation and surface temperature reduction by green roofs. Presented at the Transactions of the Asae. American Society of Agricultural and Biological Engineers, St. Joseph, Michigan, pp. 1491–1496.
Dunnett, N., Nagase, A., Booth, R., Grime, P., 2008a. Influence of vegetation composition on runoff in two simulated green roof experiments. Urban Ecosyst. 11, 385–398. doi:http://dx.doi.org/10.1007/s11252-008-0064-9.
Dunnett, N., Nagase, A., Hallam, A., 2008b. The dynamics of planted and colonising species on a green roof over six growing seasons 2001–2006: influence of substrate depth. Urban Ecosyst. 11, 373–384. doi:http://dx.doi.org/10.1007/s11252-007-0042-7.
Farrell, C., Ang, X.Q., Rayner, J.P., 2013. Water-retention additives increase plant available water in green roof substrates. Ecol. Eng. 52, 112–118.
Fassman-Beck, E., Voyde, E., Simcock, R., Hong, Y.S., 2013. 4 Living roofs in 3 locations: does configuration affect runoff mitigation. J. Hydrol. 490, 11–20.
Fioretti, R., Palla, A., Lanza, L.G., Principi, P., 2010. Green roof energy and water related performance in the Mediterranean climate. Build. Environ. 45, 1890–1904. doi:http://dx.doi.org/10.1016/j.buildenv.2010.03.001.
Getter, K.L., Rowe, D.B., Andresen, J.A., 2007. Quantifying the effect of slope on extensive green roof stormwater retention. Ecol. Eng. 31, 225–231. doi:http://dx.doi.org/10.1016/j.ecoleng.2007.06.004.
Hilten, R.N., Lawrence, T.M., Tollner, E.W., 2008. Modeling stormwater runoff from green roofs with HYDRUS-1D. J. Hydrol. 358, 288–293. doi:http://dx.doi.org/10.1016/j.jhydrol.2008.06.010.
Jim, C.Y., Peng, L.L.H., 2012. Substrate moisture effect on water balance and thermal regime of a tropical extensive green roof. Ecol. Eng. 47, 9–23. doi:http://dx.doi.org/10.1016/j.ecoleng.2012.06.020.
Klaassen, W., Bosveld, F., de Water, E., 1998. Water storage and evaporation as constituents of rainfall interception. J. Hydrol. 212–213, 36–50. doi:http://dx.doi.org/10.1016/S0022-1694(98) 200-5.
Li, Y., Babcock Jr, R.W., 2014. Green roof hydrologic performance and modeling: a review. Water Sci. Technol. 69 (4) .
Mentens, J., Raes, D., Hermy, M., 2006. Green roofs as a tool for solving the rainwater runoff problem in the urbanized 21st century? Landscape Urban Plan. 77, 217–226. doi:http://dx.doi.org/10.1016/j.landurbplan.2005.02.010.
Monterusso, M.A., Rowe, D.B., Rugh, C.L., Russell, D.K., 2004. Runoff water quantity and quality from green roof systems. Acta Hortic. 639, 369–376.
Morgan, S., Celik, S., Retzlaff, W., 2013. Green roof storm-water runoff quantity and quality. J. Environ. Eng. 139, 471–478. doi:http://dx.doi.org/10.1061/(ASCE)EE.1943-7870 (0000589).
Nagase, A., Dunnett, N., 2012. Amount of water runoff from different vegetation types on extensive green roofs: effects of plant species, diversity and plant structure. Landscape Urban Plan. 104 (3), 356–363.
Palla, A., Gnecco, I., Lanza, L.G., 2009. Unsaturated 2D modelling of subsurface water flow in the coarse-grained porous matrix of a green roof. J. Hydrol. 379, 193–204. doi:http://dx.doi.org/10.1016/j.jhydrol.2009.10.008.
Palla, A., Gnecco, I., Lanza, L.G., 2012. Compared performance of a conceptual and a mechanistic hydrologic models of a green roof. Hydrol. Processes 26, 73–84. doi:http://dx.doi.org/10.1002/hyp.8112.
Palla, A., Sansalone, J.J., Gnecco, I., Lanza, L.G., 2011. Storm water infiltration in a monitored green roof for hydrologic restoration. Water Sci. Technol. 64, 766–773. doi:http://dx.doi.org/10.2166/wst.2011.171.
Schroll, E., Lambrinos, J., Righetti, T., Sandrock, D., 2011. The role of vegetation in regulating stormwater runoff from green roofs in a winter rainfall climate. Ecol. Eng. 37 (4), 595–600.
She, N., Pang, J., 2010. Physically based green roof model. J. Hydrol. Eng. 15, 458–464. doi:http://dx.doi.org/10.1061/(ASCE)HE.1943-5584.0000138.
Simmons, M.T., Gardiner, B., Windhager, S., Tinsley, J., 2008. Green roofs are not created equal: the hydrologic and thermal performance of six different extensive green roofs and reflective and non-reflective roofs in a sub-tropical climate. Urban Ecosyst. 11, 339–348. doi:http://dx.doi.org/10.1007/s11252-008-0069-4.
Steusloff, S., 1998. Input and output of airborne aggressive substances on green roofs in Karlsruhe. In: Breuste, J., Feldmann, H., Uhlmann, O. (Eds.), Urban Ecology. Springer-Verlag, Berlin, Heidelberg, Germany.
Stovin, V., Vesuviano, G., Kasmin, H., 2012. The hydrological performance of a green roof test bed under UK climatic conditions. J. Hydrol. 414–415, 148–161. doi:http://dx.doi.org/10.1016/j.jhydrol.2011.10.022.
Stovin, V., Poë, S., Berretta, C., 2013. A modeling study of long term green roof retention performance. J. Environ. Manage. 131, 206–215.
Sun, T., Bou-Zeid, E., Ni, G.-H., 2014. To irrigate or not to irrigate: analysis of green roof performance via a vertically-resolved hygrothermal model. Build. Environ. 73, 127–137. doi:http://dx.doi.org/10.1016/j.buildenv.2013.12.004.
Sun, T., Bou-Zeid, E., Wang, Z.-H., Zerba, E., Ni, G.-H., 2013. Hydrometeorological determinants of green roof performance via a vertically-resolved model for heat and water transport. Build. Environ. 60, 211–224. doi:http://dx.doi.org/10.1016/j.buildenv.2012.10.018.
Šimu°nek, J., Šejna, M., Saito, H., Sakai, M., van Genuchten, T., 2009. HYDRUS 1D Software Package for Simulating the One-dimensional Movement of Water, Heat, and Multiple Solutes in Variably-saturated Media (No. HYDRUS-1D). Department of Environmental Sciences, University of California Riverside.
Teemusk, A., Mander, Ü., 2007. Rainwater runoff quantity and quality performance from a greenroof: the effects of short-term events. Ecol. Eng. 30, 271–277. doi:http://dx.doi.org/10.1016/j.ecoleng.2007.01.009.
Tillinghast, E., Hunt, W., Jennings, G., D'Arconte, P., 2013. Increasing stream geomorphic stability using storm water control measures in a densely urbanized watershed. J. Hydrol. Eng. 17, 1381–1388. doi:http://dx.doi.org/10.1061/(ASCE)HE.1943-5584 (0000577).
Uhl, M., Schiedt, L., 2008. Green roof storm water retention – monitoring results. 11th International Conference on Urban Drainage Edinburgh, Scotland, UK. 31, 8–15.
Van Genuchten, M.T., 1980. A closed-form equation for predicting the hydraulic conductivity of unsaturated soils. Soil Sci. Soc. Am. J. 44, 892–898.
Vanuytrecht, E., Van Mechelen, C., Van Meerbeek, K., et al., 2014. Runoff and vegetation stress of green roofs under different climate change scenarios. Landscape Urban Plan. 122 (2), 68–77.
VanWoert, N.D., Rowe, D.B., Andresen, J.A., Rugh, C.L., Fernandez, R.T., Xiao, L., 2005. Green roof stormwater retention: effects of roof surface, slope, and media depth. J. Environ. Qual. 34, 1036–1044. doi:http://dx.doi.org/10.2134/jeq2004.0364.
Villarreal, E.L., 2007. Runoff detention effect of a sedum green-roof. Nord. Hydrol. 38, 99–105. doi:http://dx.doi.org/10.2166/nh.2007.031.
Villarreal, G.E., Bengtsson, L., 2005. Response of a Sedum green-roof to individual rain events. Ecol. Eng. 25 (1), 1–7.
Volder, A., Dvorak, B., 2014. Event size, substrate water content and vegetation affect storm water retention efficiency of an un-irrigated extensive green roof system in Central Texas. Sustain. Cities Soc. 10, 59–64. doi:http://dx.doi.org/10.1016/j.scs.2013.05.005.
Voyde, E., Fassman, E., Simcock, R., 2010. Hydrology of an extensive living roof under sub-tropical climate conditions in Auckland, New Zealand. J. Hydrol. 394 (3), 384–395.
Wolf, D., Lundholm, J.T., 2008. Water uptake in green roof microcosms: effects of plant species and water availability. Ecol. Eng. 33, 179–186.
Zhang, D.-L., Lin, Y., Zhao, P., Yu, X., Wang, S., Kang, H., Ding, Y., 2013. The Beijing extreme rainfall of 21 July 2012: right results but for wrong reasons. Geophys. Res. Lett. 40, 1426–1431. doi:http://dx.doi.org/10.1002/grl.50304.
Zhang, S., Guo, Y., 2013. An analytical probabilistic model for evaluating the hydrologic performance of green roofs. J. Hydrol. Eng. 18 (1), 19–28.

Further reading

DiGiovanni et al., 2010 K. DiGiovanni , S. Gaffin , F. Montalto , Green Roof Hydrology: Results from a Small-Scale Lysimeter Setup American Society of Civil Engineers Bronx, NY 2010;

Lundholm et al., 2010 J. Lundholm , J.S. MacIvor , Z. MacDougall , M. Ranalli . Plant species and functional group combinations affect green roof ecosystem functions PLos One 2010; 5: (3) e9677